Effect of stator blades on the startup dynamics of a vertical axis wind turbine.

ASIM, T., SINGH, D., SIDDIQUI, M.S. and MCGLINCHEY, D.

2022

energies

Article

Effect of Stator Blades on the Startup Dynamics of a Vertical Axis Wind Turbine

Taimoor Asim [1] Dharminder Singh [2] Muhammad Salman Siddiqui [3] * and Don McGlinchey [2]

[1] School of Engineering, Robert Gordon University, Aberdeen, UK, AB10 7GJ; t.asim@rgu.ac.uk
[2] Department of Mechanical Engineering, Glasgow Caledonian University, Glasgow, UK, G4 0BA; dharminder.singh2@rgu.ac.uk
[3] Faculty of Science and Technology, Norwegian University of Life Sciences, 1430 Ås, Norway; muhammad.salman.siddiqui@nmbu.no
* Correspondence: muhammad.salman.siddiqui@nmbu.no; Tel.: +47 486 28 035

Abstract: Vertical Axis Wind Turbines (VAWTs) are omni-directional, low-cost, low-efficiency wind power extractors. A conventional drag-based VAWT consists of multiple thin rotor blades with a typical peak Tip Speed Ratio (λ) of < 1. Their lower cut-in speed and maintenance cost make them ideal for power generation in urban environments. Numerous studies have been carried out analysing steady operation of VAWTs and quantifying their performance characteristics, however, minimal attention has been paid to their start-up dynamics. There are a few recent studies in which start-up dynamics of lift-based VAWTs have been analysed but such studies for drag-based VAWTs are severely limited. In this study, start-up dynamics of a conventional multi-blade drag-based VAWT have been numerically investigated using a time-dependant Computational Fluid Dynamics (CFD) solver. In order to enhance the start-up characteristics of the drag-based VAWT, a stator has been integrated in the design assembly. The numerical results obtained in this study indicate that an appropriately designed stator can significantly enhance the start-up of a VAWT by directing the flow towards the rotor blades, leading to higher rotational velocity (ω) and λ. With the addition of a stator, the flow fields downstream the VAWT becomes more uniform.

Keywords: Vertical Axis Wind Turbine (VAWT); Computational Fluid Dynamics (CFD); Start-Up Dynamics; Dynamic Meshing; Tip Speed Ratio

Citation: Lastname, F.; Lastname, F.; Lastname, F. Title. *Energies* **2021**, *14*, x. https://doi.org/10.3390/xxxxx

Academic Editor: Firstname Lastname

Received: date
Accepted: date
Published: date

1. Introduction

In order to reduce dependency on fossil fuels and to tackle climate change, the use of renewable energy sources, especially wind energy, has become very popular in the past few decades. Wind energy is harnessed using wind turbines by capturing the kinetic energy from the wind. This is achieved through wind induced rotation to the wind turbine blades, and the generator shaft, to produce electricity. Depending on the axis of rotation, wind turbines can be classified into Vertical Axis Wind Turbines (VAWTs) and Horizontal Axis Wind Turbines (HAWTs) [1,2]. HAWTs are a popular choice for harnessing wind energy in mid to large scale wind farms [3], which are built on vast, open locations where the turbines can get sustained wind velocities above turbines' cut-in speed. They also need a yaw control mechanism so that the turbine is always facing the direction of the wind for maximum power extraction [4]. Therefore, they have a high utilisation coefficient. In urban locations however, the wind speed and direction is highly non-uniform, making VAWTs advantageous in these locations, as they have a much lower cut-in speed and are omni-directional, thus, not requiring a yaw control mechanism [5]. Apart from the simplified design of VAWTs, research studies [6-8] have shown that they can be installed much closer to each other since they can also extract power from the wake generated by the turbines upstream.

1.1 Rationale to carry out this study

Irrespective of their cut-in speeds, the start-up speed of wind turbines, both HAWTs and VAWTs, is a function of turbine size, shape and wind speed. VAWTs are generally considered to have lower start-up speeds, not particularly because of their shape, rather their smaller size compared to HAWTs. Thus, for bigger VAWTs with potentially higher power generation, their start-up speeds become an important contributing factor towards their commercial viability. It is a well-known fact that VAWT's peak Tip Speed Ratio (λ) is much smaller than HAWTs [9], thus, for same size and wind speed, VAWTs' rotational velocity (ω) is lower than HAWTs'. This is probably the primary limiting factor VAWTs' industry is currently experiencing in terms of upscaling. In order to address these industrial challenges, i) the start-up dynamics of VAWTs must be fully understood and analysed, and ii) technologies must be developed to decrease VAWTs' start-up speeds (or increase their ω at the same start-up speeds). We aim to address both these challenges in the present study however, we must first review the published literature that deal with the start-up dynamics of wind turbines, focusing on VAWTs.

1.2 Rationale for choosing Drag-based VAWTs

There are two main types of VAWTs i.e. lift-based and drag-based, commonly known as Darrieus and Savonius VAWTs [10]. Most of the published literature deals with lift-based VAWTs, however, the present study analyses drag-based VAWTs. The primary reason for choosing drag-based VAWTs over more commonly studied lift-based VAWTs is the fact that the manufacturing and disposal of lift-based VAWTs' rotor blades is a significant challenge. These are the same challenges faced by the HAWT industry. Thus, the rotor blades of lift-based VAWTs are quite expensive (because of their NACA profile) and there are very limited number of blade manufacturers (e.g. Siemens, GE, Bureau Veritas) that can deliver mid to large scale blades. Moreover, currently these blades are disposed in landfills, causing potentially considerable environmental impact. With 40,000 non-recyclable composite blades going to be disposed of in the next 10 years in Europe alone, the authors believe a more viable option for technology development is drag-based VAWTs, where the blades are made out of inexpensive recyclable materials (e.g. steel, aluminium) and their shape is much simpler (cup shaped) compared to lift-based VAWTs. It is however noteworthy that most of the published literature deals with the start-up dynamics of lift-based VAWTs, a review of which is presented below.

1.3 Start-up Dynamics of Lift-based VAWTs

Hill et al [11], to the authors' best knowledge, were the first to report the start-up dynamics of VAWTs. They carried out experimental investigations on a H-rotor lift-based VAWT model in an open jet configuration wind tunnel. The results obtained show that there are four stages of start-up process. The first stage is the linear acceleration where the turbine rotor accelerates from rest to a λ value of just above 1. The second stage is called the first plateau where the turbine almost stops accelerating and operates at roughly a constant speed ($\lambda \sim 1.2$). The third stage of start-up is the rapid acceleration to $\lambda \sim 3$. The last stage of the start-up is the second plateau, or steady operation of the VAWT at $\lambda \sim 3$. The plateaus have been referred to as 'dead band' by some researchers [12-13], during which the turbine cannot accelerate because of negative torque [14]. However, Hill et al's [11] results show that if λ can increase gradually to ~ 1.5, then the VAWT can accelerate rapidly to its maximum steady operation. Asr et al [15] conducted numerical investigations to study the start-up characteristics of a H-rotor lift-based VAWT, having NACA0018 airfoils for the blades, using flow induced rotation approach. The numerically predicted results have been validated against the published experimental data of Rainbird [16] and Hill et al [11]. Asr et al [15] have also noticed four stages in the start-up of the turbine, however, carrying further investigations, they found out that the turbines with NACA0015 and NACA0022 airfoils were not able to accelerate past the dead band region.

They also investigated the effect of changing the pitch angle and found that inward pitch angles worsened the performance of NACA0018 airfoils, but applying small outward pitch angles (1.5° - 3°) improved the start-up performance, resulting in a decrease of 23% - 32% in start-up time. Using higher outward pitch angles eliminated the plateau region but increased the time the turbine took to reach its peak ω.

Zhu et al [17-18] and Sun et al [19] carried out a number of numerical investigations on the start-up dynamics of H-rotor lift-based VAWT. It has been reported that fluctuations in the wind velocity influences the start-up of VAWTs [17]. The fluctuation frequency is found to have negligible effect of the start-up, while large fluctuation amplitudes can degrade the start-up performance of VAWTs. Zhu et al [18] further investigated the effects of rotational friction ratio on the power extraction capability of the VAWT. It has been found that smaller rotational friction ratio can benefit the power extraction at lower wind speeds, while larger rotational friction ratio is beneficial at higher wind speeds. Sun et al [19] then investigated the effects of number of blades (3 and 5) and blade pitch angles (-4° to +4°) on the start-up of VAWTs. It has been found out that both these parameters have negligible effects on the start-up of the VAWTs at lower wind speeds, while at higher wind speeds, a greater number of blades and larger blade pitch angles aid the start-up process. Zhu et al [20] also agree with the findings of Sun et al [19], with the addition that the blade solidity also plays an important part in the start-up of the VAWTs. It has been reported that with lower solidity, more power extraction is possible however, the start-up is delayed, and vice versa.

Some researchers have reported that VAWTs face difficulty in self-starting without any external assistance [1,21]. Solidity of a VAWT is an important factor that strongly affects its self-starting ability, optimal λ and maximum Power Coefficient (C_P) [22]. Hill et al's [11] study shows that the turbine with solidity of 0.33 can self-start under a wind speed of 6 m/s. Dominy et al [23] have found that under lightly loaded conditions, the ability of two-bladed lift-based turbines to self-start depends on the angular orientation of the blades but a three-bladed turbine can start from any orientation. It can thus be concluded that the start-up of lift-based VAWTs are dependent on the initial orientation of the rotor blades. Moreover, Tigabu et al [24] numerically analysed the effects of turbine inertia on the start-up characteristics of a H-rotor hydrokinetic turbine. They have noticed that if the turbine starts from rest with no load condition, it overshoots steady λ point before coming back to the steady operation of the VAWT i.e. steady λ. Goude and Lundin [25] found that as the turbine inertia reduces, the start-up time decreases, however, at higher inertia, the overshoot decreases and start-up goes through the four stage start-up process described by Hill et al [11].

1.4 Start-up Dynamics of Drag-based Turbines

Zhao et al [26] investigated the start-up process of a two-bladed drag-based hydrokinetic turbine using experimentation and numerical investigations, considering the effects of initial azimuthal angles. It has been found that the static torque coefficient changes significantly with the azimuthal angle and therefore, the starting position of the rotor is important for successful start-up of the turbine. Apart from the dead band azimuthal positions where the turbine experiences a negative torque, it has been found that some positions, where the static torque on the rotor is positive, the rotor could not start successfully. The start-up process of drag-based turbines has been divided into two stages i.e. an initial acceleration and the transition stages. At the end of the transition stage, the angular velocity fluctuates periodically over a small range representing a stable operation of the rotor. Kang et al [27] have carried out further investigations with the aim to improve the start-up of the hydrokinetic turbine considered by Zhao et al [28]. They developed a two-stage hydrokinetic turbine (top and bottom configuration) and noticed a similar pattern of start-up to single stage turbine. It has been reported that the angular speed of the rotor accelerated smoothly to the stable state and the fluctuations in the stable state reduced considerably. The start-up time for the two-stage rotor has been shown to be lower than the single stage rotor. Mu et al [29] have carried out experimental and numerical investigations on the start-up and steady performance of two-bladed drag-based VAWTs, with conventional (straight) and spiral blades. It has been reported that for certain azimuthal angles, the conventional drag-based VAWT could not start, but the spiral blade VAWT did, at all azimuthal angles. Like Zhao et al [26] and Kang et al [27], rapid initial acceleration and then transition to steady operation of the VAWT have been reported, with peak ω increasing as wind speed increases. It has also been recorded that the spiral blade VAWT generated significantly higher torque. After conducting a review of the published literature regarding the start-up dynamics of VAWTs, the review of research studies on the performance characterisation of VAWTs, with and without stator blades, is presented below.

1.5 Performance Characterisation of VAWTs with and without Stator

Altan and Atilgan [30] placed a curtain arrangement as a simple wind deflector in front of a drag-based rotor. It has been found that at the curtain's optimum angle, C_P increases by 38 %, however, the use of the curtain reduced the operational range of the rotor. Golecha et al [31] showed that a properly placed deflector plate can increase VATW's C_P by 50 % compared to a rotor with no deflector. The reason for the improvement in performance of the VAWT due to curtain is that shielding the returning blade with a deflector plate reduces the flow resistance experienced by the blade, which reduces negative torque. The same principle was utilised by Alizadeh et al [32] to increase the performance of a VAWT where they shielded the returning blade of the turbine rotor by a quadrant barrier. Pope et al [5] investigated the effects of vanes on C_P of a Zephyr VAWT which includes stator vanes with reverse winglets around the rotor. This design has a high solidity, due to which, it performs well at low λ but at higher wind speeds, the peak performance is limited. Hayashi et al [33] showed that using guide vanes in front of a drag-based rotor increases the average Torque Coefficient (C_T) at low λ. They also tested a stacked configuration of the turbine with three stages. Golecha et al [31] conducted experiments on similarly stacked two stage and three stage configurations, resulting in a decrease in C_P as compared to single stage rotor with the same aspect ratio. However, for multi-stage turbines, the performance improved when a deflector plate is placed in front of the rotors.

Su et al [34] investigated the effect of V-shaped blades to improve the aerodynamic performance of a conventional straight bladed lift-based turbine. High-fidelity 3D Computational Fluid Dynamics (CFD) based simulations were carried out and the results obtained indicate 20 % increase in C_P when V-shaped blades are used. Reduction in torque fluctuation has also been observed, resulting in more stable performance of the VAWT. Jiang et al [35] numerically investigated the effects of blade tip shape and supporting strut on a large turbine model with the aim to reduce blade tip vortex and to optimise the structure of the turbine for enhanced performance. Roy and Saha [36] developed a new blade profile for a drag-based turbine from a series of experimental studies on Bach and Benesh type turbines by modifying geometric arcs, overlapping distances and dimensions of blade profiles. Their design show improved performance as compared to other blade profile shapes such as semi-circular and semi-elliptical. It is clear that the use of a deflector (or stator) improves the performance characteristics of VAWTs however, as most of these studies have been carried out using prescribed ω, flow induced rotation of the turbines has not been investigated [37], which may have a significant effect on the performance of the turbines. We aim to numerically investigate flow induced rotation of drag-based VAWT, with and without stator, focusing on the start-up dynamics of the VAWTs.

2. Numerical Modelling of the Drag-based VAWT

This section details the various steps involved in developing the numerical model of the drag-based VAWT, with and without the stator.

2.1. Geometry of the VAWT and the Flow Domain

The VAWT considered in the present study comprises of 12 rotor blades. This is the same VAWT that Gareth [38] initially developed and analysed, and then the authors carried out a number of empirical and numerical investigations on it over a number of years [39-44]. The full-scale VAWT (with stator) is shown in figure 1(a). A Computer Aided Design (CAD) model of the same VAWT has been created, as shown in figure 1(b) (not including the stator). The inner and outer diameters of the rotor are 1 m and 1.4 m respectively, while the height of the VAWT is 1 m.

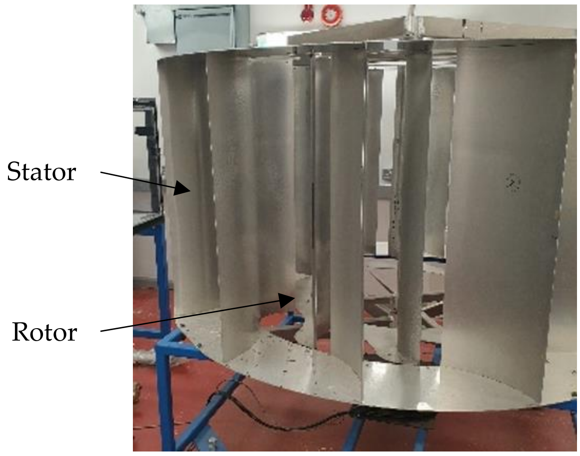

(a)

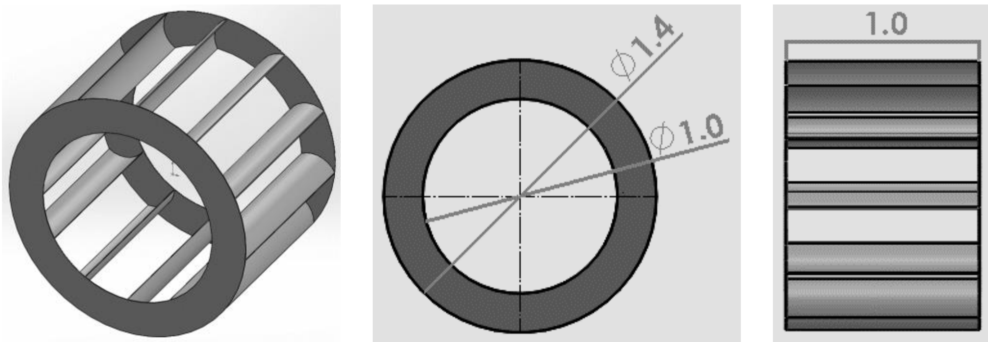

(b)

Figure 1. (a) Real-world VAWT model (with stator) (b) CAD model of the VAWT without stator

For the purpose of carrying out Computational Fluid Dynamics (CFD) investigations on the start-up dynamics of the VAWT, the CAD model has been converted into the numerical model using a widely used commercial CFD package Ansys® Fluent. It is important to point out here that although the CAD model of the VAWT shown in figure 1(b) is 3D, we have extracted only a 2D VAWT model from it for the purpose of numerical investigations. The justification for not considering the 3D VAWT model is its computational expense and the availability of computational resources. A typical 3D VAWT model, for steady-state CFD investigations, comprises of > 5×10^6 mesh elements [45]. For time-dependant CFD investigations (as in this study), where the aim is to capture the start-up dynamics of the VAWT, the number of mesh elements required is significantly higher. Additionally, instead of running the numerical simulations for a few thousand iterations, the simulations should be performed over a few million iterations (details in sections below), which is computationally prohibitive; each simulation in the present work took 4 months. Other computational-based research studies carried out on the start-up dynamics have also considered 2D models [15,17-20,24-25]. Thus, the choice of considering a 2D model is justified.

The 2D numerical models of both the VAWTs considered in the present study i.e. with and without the stator, are shown in figure 2(a). Note: the stator also comprises of 12 blades and has an outer diameter of 2 m [38]. These VAWT models are placed inside a rectangular flow domain, having a length of 15 m and a height of 6 m, as shown in figure 2(b). In order to generate a controlled mesh in the near-wall and wake regions of the VAWTs, where the flow is expected to be more complex in nature and changing fast w.r.t. time, an inner domain has been created, having a length of 10 m and a height of 2.5 m. Asim et al [10] have previously shown that using two domains, having sizes specified here, for multi-blade drag-based VAWTs, help in capturing the complex flow features accurately.

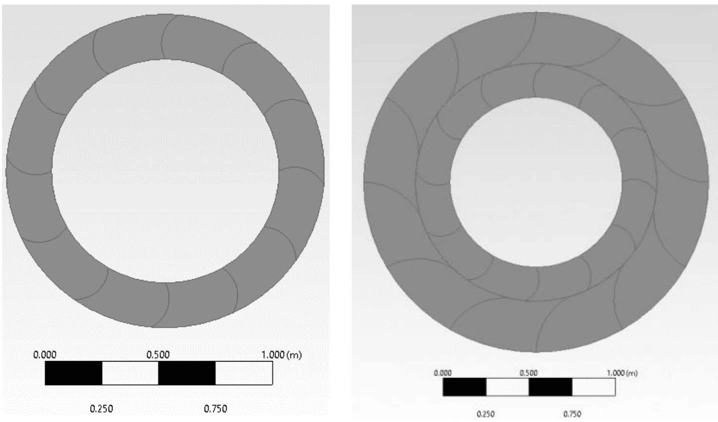

(a)

(b)

Figure 2. (a) 2D models of the VAWTs with and without stator (b) Flow domain of the VAWTs

2.2 Meshing of the Flow Domains

In order to generate an appropriate mesh within the flow domain, three different sizing have been specified. For the outer domain, a mesh size of 40 mm has been generated. For inner domain and the core region of the VAWT, a sizing of 20 mm has been specified, while for the rotor (and stator) region, mesh elements of size 10 mm have been generated. The resulting mesh within the flow domain is shown in figure 3. Asim et al [10] specified size of 100 mm to the outer domain, 30 mm to the inner domain and 15 mm to the blades region for conducting steady performance analysis of this VAWT (with stator). We have further decreased the size because we have to capture more intrinsic flow details during the start-up of the VAWTs. Moreover, the mesh elements generated in the present study are all quadrilaterals, with enhanced mesh structure. The resulting number of mesh elements is ~ 2 x 10^5.

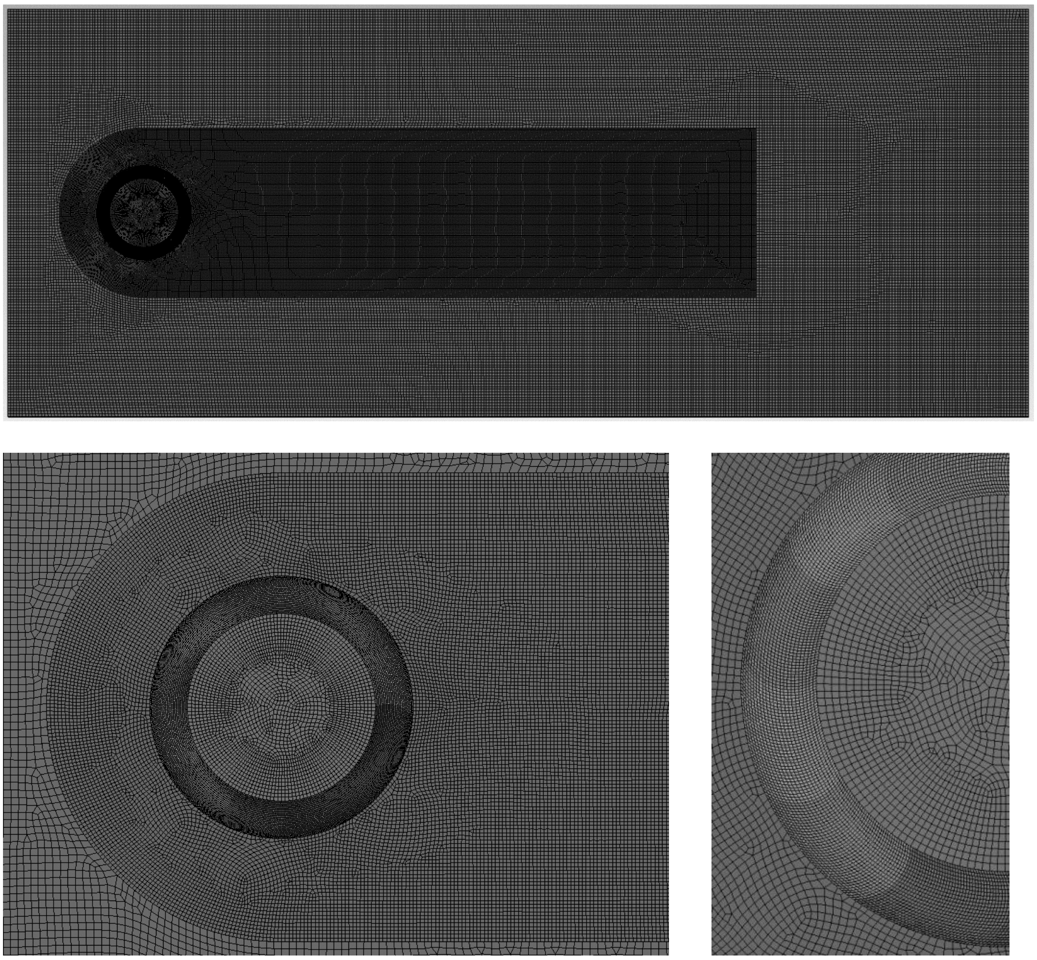

Figure 3. Spatial discretisation of the flow domains

It is a well-known fact that in any CFD based study, the appropriateness of the mesh being used is crucial for the accuracy of the results obtained [46]. There is quite a straight-forward approach used for this when analysing steady-state performance of turbomachines, which is known as mesh independence study [47]. This approach, however, is not suitable for time-dependant solutions, especially where the length scales of energy carrying eddies are expected to change significantly during the numerical calculations. The suitability of a mesh is dependent on how well it can capture the smallest length scale in the flow domain. As wall effects are dominant in case of VAWTs, we need to ensure that near-wall mesh density is adequate. Thus, we define a parameter that relates cell-base length scale to its height as a Custom Field Function (CFF). Equation (1) defines the ratio of cell-base length to the cell's height (φ) as [10]:

$$\varphi = \frac{\sqrt{A}}{2\,y} \qquad (1)$$

where A is the element's face area (in m²) and y is the wall distance (in m). Low values of φ are considered appropriate to capture small eddies in near-wall regions (typically < 10). Figure 4 depicts the spatial variations in φ at time 0.0382s i.e. very early on in the start-up of the VAWT. It can be seen that φ values are higher in the near-wall regions, as expected, but less than 10. In comparison with the stator blades, the rotor blades have slightly higher φ, due to their rotation. Hence, it can be concluded that the mesh considered in the present study is appropriate to capture the small-scale eddies accurately.

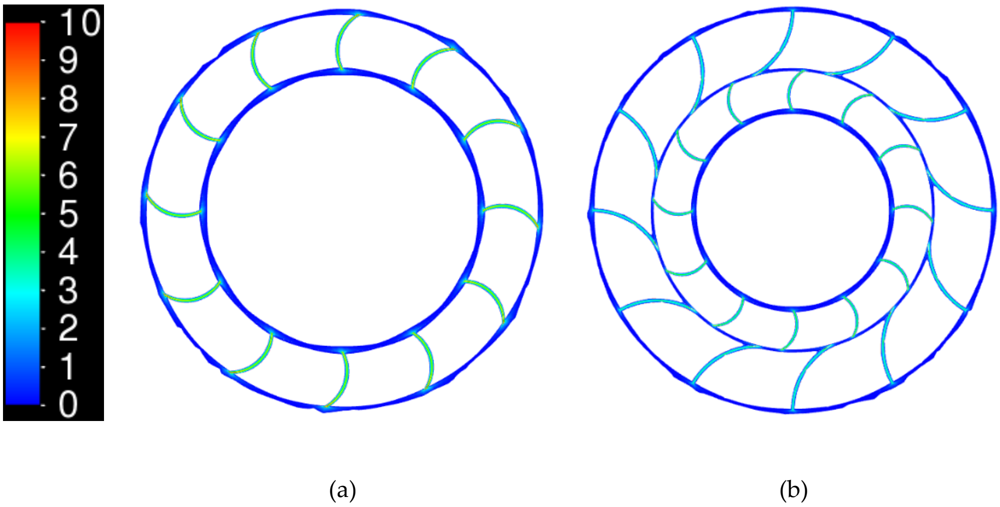

Figure 4. Variations of φ in the near-wall regions of the VAWT (a) without stator (b) with stator

2.3 Boundary Conditions and Flow Governing Equations

The boundary conditions specified in the present study are summarised in Table 1. The UK annual average wind speed of 4.2 m/s has been considered as the inlet flow velocity. The outlet of the flow domain has been specified with atmospheric pressure condition. The top and bottom edges of the outer flow domain have been specified as symmetries, to avoid wall effects [24]. Stator blades are stationary, as expected, while the rotor blades are moving. The modelling of rotor blades' rotational motion is discussed in the next section.

Table 1. Boundary conditions specified to the numerical model

Boundary	Type	Value
Inlet	Velocity	4.2 m/s
Outlet	Pressure	0 Pa,g
Top and Bottom edges of the Outer Domain	Symmetry	
All edges of the Inner Domain	Sliding Interfaces	
Stator Blades	Stationary Wall	No-slip
Rotor Blades	6DOF	No-slip

Based on the inlet flow velocity of 4.2 m/s, air density and dynamic viscosity of 1.225 kg/m³ and 1.789 x 10^{-5} Pa.s, the Reynolds number (Re) has been calculated to be 4 x 10^5 for the VAWT without stator (and 5.7 x 10^5 for the VAWT with stator). Hence, the flow is turbulent, and the corresponding mass conservation equation is:

$$\frac{\partial u_i}{\partial x_i} = 0 \quad (2)$$

For momentum conservation, we employ the conventional Reynolds Averaged Navier-Stokes equation (URANS), which can be expressed as [48]:

$$\frac{\partial \bar{u}_i}{\partial t} + \frac{\partial}{x_j}\left(\overline{u_i u_j}\right) = -\frac{1}{\rho}\frac{\partial \bar{p}}{\partial x_i} + \frac{\partial}{x_j}\left[\upsilon\left(\frac{\partial \bar{u}_i}{\partial x_j} + \frac{\partial \bar{u}_j}{\partial x_i}\right)\right] + \frac{\partial}{x_j}\left(-\overline{\acute{u}_i \acute{u}_j}\right) \quad (3)$$

where u_i and u_j are velocity vectors, ' represents fluctuations, ¯ represent mean, p is the pressure and υ is the turbulent kinematic viscosity (or eddy viscosity). $-\overline{\acute{u}_i \acute{u}_j}$ is the Reynolds stress. In order to relate the eddy viscosity (υ) to Reynolds stress, we employ the Spalart-Allmaras turbulence model that comprises of an eddy viscosity transport equation, in order to close equation (3). Sun et al [19] also employed the Spalart-Allmaras model while investigating start-up dynamics of lift-based VAWTs, as it is widely used in aerodynamics and turbomachinary applications. The transport equation for the turbulent kinematic viscosity in the Spalart-Allmaras model is expressed as [49]:

$$\frac{\partial}{\partial t}(\rho\upsilon) + \frac{\partial}{\partial x_i}(\rho\upsilon u_i) = A_\upsilon + \frac{1}{\sigma_\upsilon}\left[\frac{\partial}{\partial x_j}\left\{(\mu + \rho\upsilon)\frac{\partial \upsilon}{\partial x_j}\right\} + B\rho\left(\frac{\partial \upsilon}{\partial x_j}\right)\right] - C_\upsilon \quad (4)$$

where A_υ is the production and C_υ is the destruction of υ, σ_υ and B are the constants.

2.4 Six Degree of Freedom (6DOF) Solver

For modelling flow induced rotation of the rotor blades, a Six Degree of Freedom (6DOF) solver has been employed in the present study. In 6DOF solver, the aerodynamic forces and moments applied by the wind on the rotor blades are computed numerically, and then used to determine (and apply) the resulting angular rotation to the rotor blades, along their centre of gravity. Based on Newton's second law, we know that the torque applied (T) is expressed as:

$$T = I\alpha \quad (5)$$

where I is the mass moment of inertia of the rotor (in $kg.m^2$) and α is its angular acceleration (in rad/s^2). The real-world VAWT shown in figure 1(a) is made out of cold rolled sheets of aluminium, having a wall thickness of 0.5 mm. Based on VAWT's dimensions, I of the rotor has been calculated as 12.93 $kg.m^2$, and specified in the 6DOF solver. In the present study, we have not considered the generator load on the VAWT, thus, the angular velocity (ω) of the rotor keeps on increasing ($\alpha > 0$) till average $T \rightarrow 0$. There will still be fluctuations in T across 0 after the VAWT has reached steady operation due to the cyclic variations. Once T has been computed at a particular time stamp (t), the angular position of the rotor (θ) is updated according to [19]:

$$\theta^{i+1} = 2\theta^{i} - \theta^{i-1} + \frac{\omega}{I}\,\Delta t^2 \quad (6)$$

2.5 Temporal Resolution

An important parameter in equation (6) is the change in time stamps (Δt), which is more commonly known as the time step size. We know that during the start-up of VAWTs, as t increases, ω also increases, till the steady operation of the VAWT is achieved. Published literature on the start-up dynamics of VAWTs [18-19,24] use a fixed value of Δt in seconds. The authors believe that this is not an appropriate approach because ω keeps on increasing during the start-up. Using a fixed Δt in seconds can potentially not capture the small-scale eddies, leading to inaccurate flow fields and thus, the torque applied on the rotor (T) and eventually, the angular position of the blades (θ). Thus, a more appropriate methodology needs to be adopted for time advancement, which can take into account the variations in the flow field. In the present study, we use the Courant Number (C_L) for this purpose, which can be expressed as [50]:

$$C_L = |U|\frac{\Delta t}{\Delta x} \quad (7)$$

where |U| is the flow velocity magnitude (in m/s) and Δx is the distance between neighbouring mesh elements (in m). C_L is a dimensionless number that basically represents the amount of time a flow particle stays within a mesh element. C_L should ideally be < 1, but that is computationally very expensive. In the present study, we use $C_L = 1$.

Specification of an appropriate C_L does not mean that further checks on its suitability are not required, especially during the start-up phase. Thus, in the present study, we define a CFF as:

$$\tau = \frac{V^{\frac{1}{3}}}{|U|} \quad (8)$$

where V is the cell volume (in m^3). We need to ensure that Δt we obtain by using $C_L = 1$ is less than τ. At t = 0.0382s (very early on during the start-up of VAWTs), Δt for VAWT without stator is 0.000082s and for the VAWT with stator is 0.000047s. We set these as the lower limit and show the variations in τ in figure 5. It can be seen that there are no data gaps (unfilled areas) in both the cases, confirming that the choice of C_L is appropriately capturing small-scale eddies.

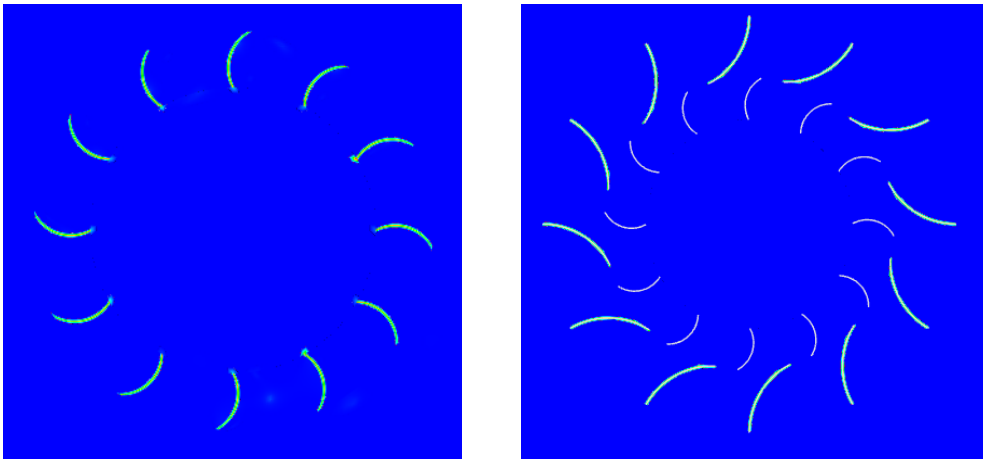

(a) (b)

Figure 5. Variations of τ in the vicinity of VAWT (a) without stator (b) with stator

3. Results and Discussions

3.1 Start-up Dynamics of VAWT without Stator

In this section, we present detailed analysis of flow induced rotation of the first VAWT model considered in the present study i.e. VAWT without Stator. Firstly, the time-dependant rotation of the VAWT has been discussed, followed by the variations in the flow fields (pressure and velocity) in the vicinity of the VAWT. Note: both the VAWT models have been run for 100s to ensure that steady rotational speed is obtained. In terms of time steps, this means that both the simulations have been run for more than 6×10^5 time steps.

Figure 6 depicts the time-dependant rotation of the VAWT without Stator, where figure 6(a) shows the angular rotation (θ in °) while figure 6(b) shows the rotational speed of the VAWT (ω in rpm). It can be seen in figure 6(a) that, starting from t = 0s, as incident air exerts force on the rotor blades, they start to rotate about their central axis. As time progresses, the rotation of the VAWT increases till 360° or one revolution. Rotating further, it can be seen that θ decreases from 360° to 0°, which doesn't mean that the VAWT rotates in the opposite direction; it just completes another full revolution in normal direction of operation. The first revolution of the VAWT is completed in 4.86s, while the second revolution takes 2.38s, which is less than half the time taken to complete the first revolution (because the VAWT is constantly picking up speed). The next two revolutions take 2s and 1.84s respectively. The time taken to complete a full revolution keeps on decreasing as the VAWT's rotational speed keeps on increasing. During the first 100s of operation, the VAWT undergoes ~ 60 full revolutions. It is important to note here that figure 6(a) provides information on the angular rotation of the VAWT but doesn't provide explicit information on when the VAWT reaches a steady/constant rotational speed. Moreover, the information provided in figure 6(a) remain the same (qualitatively) for all different types of turbomachines.

Figure 6(b) depicts time-dependant variations in the rotational speed of the VAWT. There are three distinct observable regions in figure 6(b). It can be seen that starting from initial position at t = 0s, the VAWT's rotational speed starts to increase almost linearly till 9.4s. By this time, the rotational speed of the VAWT reaches 32 rpm. From 9.4s till 23s, the rate of increase in the rotational speed of the VAWT decreases. By 23s, the VAWT has achieved its maximum rotational speed of 37.8 rpm. From 23s onwards, the rotational speed of the VAWT remains constant. There are a number of interesting observations and statistics that we need to analyse here in order to better understand the start-up dynamics of the VAWT. Figure 6(b) clearly demonstrates the differences between drag-based and lift-based VAWTs. For lift-based VAWTs, it has been observed in a number of recent research studies [11,15-16,19-20] that there are four distinct zones associated with the start-up of the VAWT. These are i) linear acceleration, ii) first plateau (constant ω), iii) second linear acceleration, and iv) second plateau. Please note that here we have not considered the transition zones from linear accelerations to the plateaus; if we include these then there are six start-up zones. For the drag-based VAWT considered in the present study, we observed i) linear acceleration, and ii) plateau only (again disregarding the transition; for better comparison with lift-based VAWTs). We believe that we have run the simulations for long enough time to ensure that if a second acceleration existed, it would have been appropriately captured. Moreover, in comparison with the work carried out by Tigabu et al [24] on lift-based hydro turbines, where they noticed an additional zone i.e. offshoot, which was a continuation from linear acceleration past the maximum rotational speed, we did not experience any such offshoot in case of drag-based turbine. In the present case, the VAWT completed 12 full rotations before reaching its maximum/peak rotational speed of 37.8 rpm in 23s). It would be also useful to know the local ω values at certain key time stamps. After 5s of operation, ω = 22.3, which is 59 % of the maximum ω. After 10s of operation, ω = 32.6 (86 % of maximum) and at t = 20s, ω = 27s (98 % of maximum), which is in-line with our categorisation of the zones associated with the start-up of the VAWT.

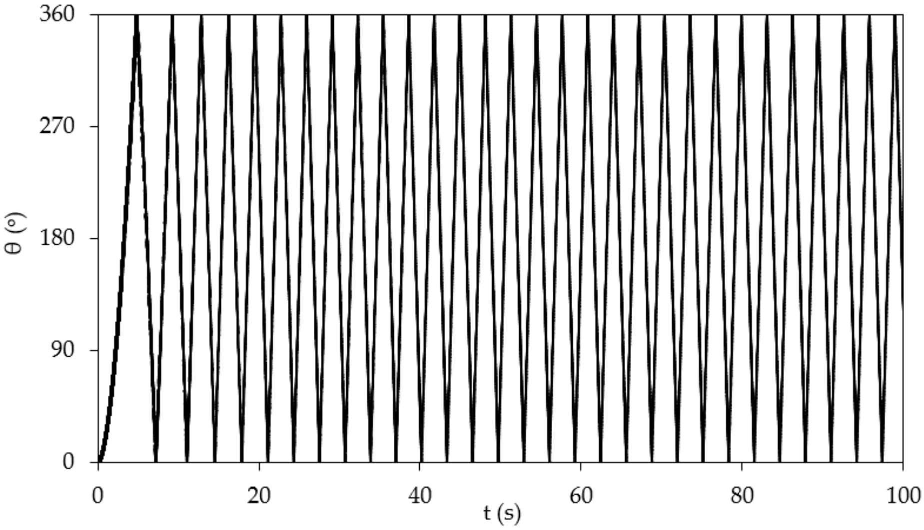

(a)

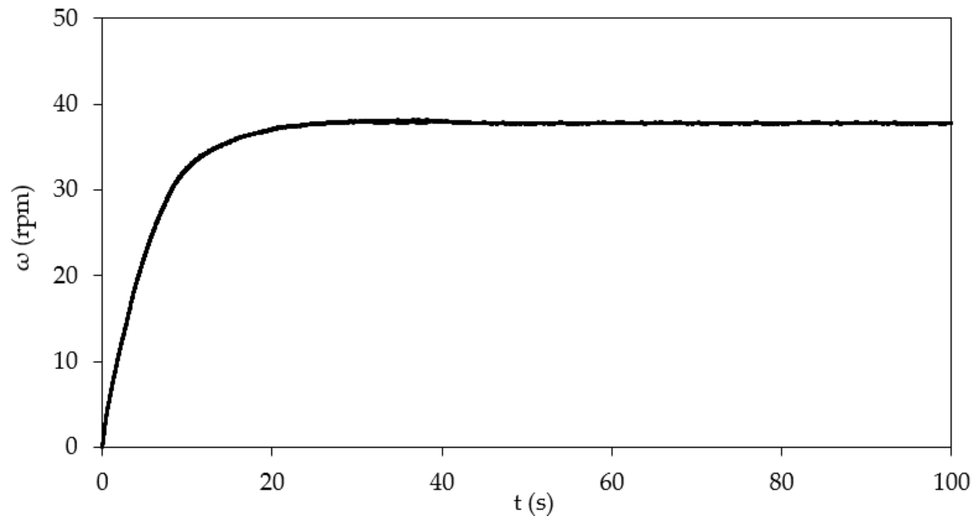

(b)

Figure 6. Rotational characteristics of the VAWT without stator

After analysing the rotational behaviour of the VAWT during its start-up, it is beneficial to study the flow fields in the vicinity of the VAWT. Thus, figure 7(a) depicts the static gauge pressure (in Pa), while figure 7(b) depicts the flow velocity magnitude (in m/s) within the flow domain. Please note that in all the flow fields presented in the present study, the flow of air is from left to right in the figures. The flow fields have been obtained at t = 5s, 10s, 15s, 20s and 25s respectively, where the first two time stamps (t = 5s and 10s) represent the linear acceleration zone, the next two (t = 15s and 20s) represent the transition zone, while the last time stamp (t = 25s) represent steady operation of the VAWT at its maximum ω. For effective comparison purposes, the scale of the variations, both in pressure and in velocity, have been kept the same for all the different time stamps considered here. It can be seen in figure 7(a) that the pressure is higher on the windward side (upstream), while it is relatively lower on the leeward side (downstream) of the VAWT, as expected [40-45]. This trend remains the same irrespective of the time stamps considered. Upon impinging the rotor blades upstream, the air pressure increases up to 40 Pa,g, (on the pressure side of the blades) which remains roughly the same for all the time stamps. On the suction side of these blades, the pressure is weakly negative. The flow detachment from the top and bottom of the VAWT (in the figure) is visible, generating local flow recirculation zones (possibly vortices). Due to the different orientation of the blades at the top and bottom, the frequency and size of these recirculating zones is different; on the top side of the VAWT, because the blades' curvature is in the direction of flow, the recirculation zones are fewer in number but bigger in size, while on the bottom side, the number of these local flow structures is more and they are smaller in size, leading to asymmetric flow on either side of the VAWT. In between the top blades, low-pressure zones start to develop during the linear acceleration phase of the start-up (t = 5s and 10s). The pressure in these zones drop further during the transition phase (t = 15s and 20s), and is then maintained during the steady operation of the VAWT (t = 25s).

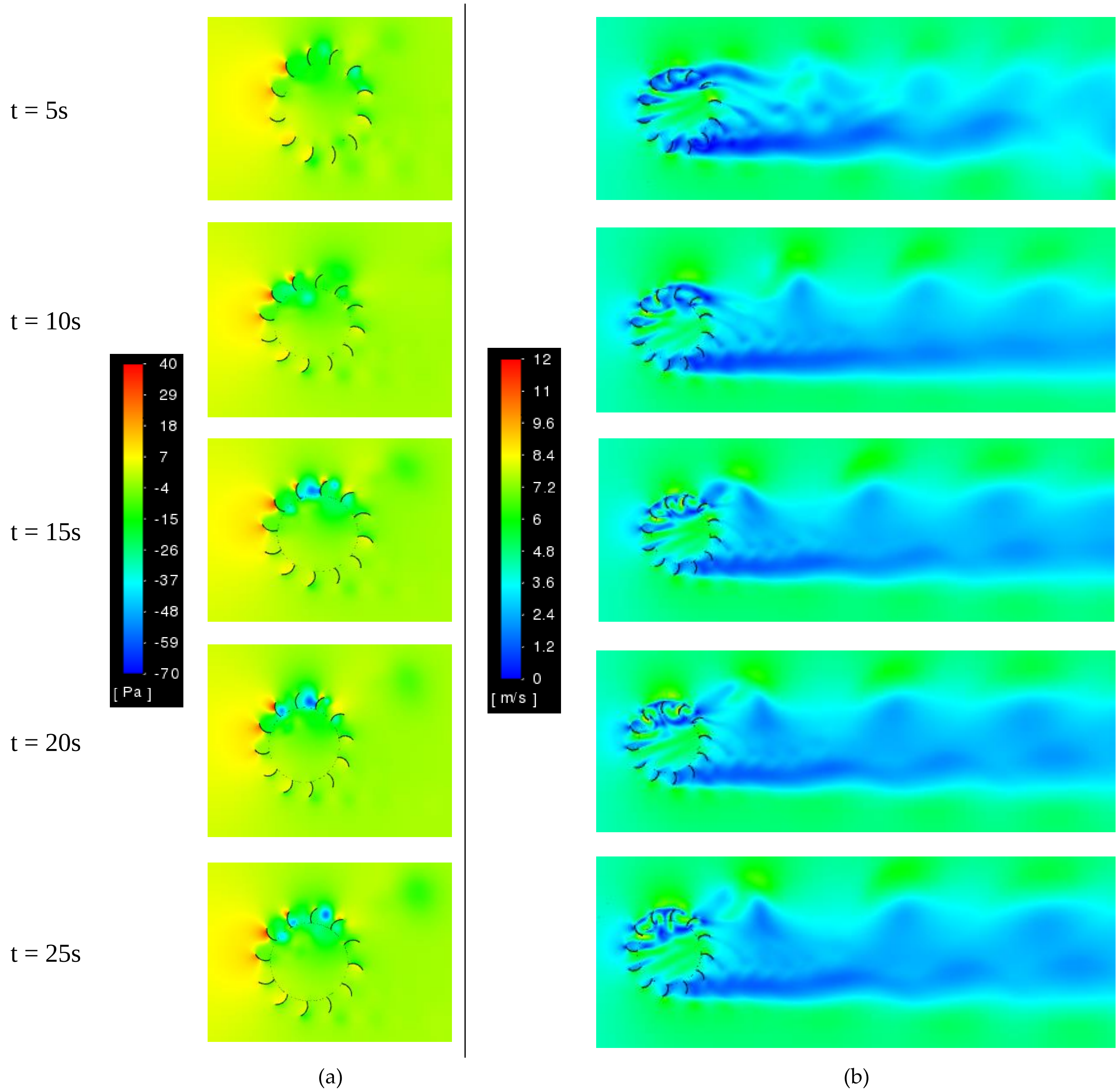

Figure 7. (a) Static gauge pressure and (b) flow velocity magnitude variations in the vicinity of the VAWT without stator

While the pressure field provides valuable information in the near-wall (blades) regions of the VAWT, the velocity field shown in figure 7(b) highlights the local flow characteristics downstream the VAWT, including the wake region. The asymmetry discussed above on either side of the VAWT is clearly visible here. It is important to point out over here that such local time-based flow field analysis of VAWTs, where rotation is induced by the flow, is very scarce in the published literature and thus, comparative analysis with, for example lift-based VAWTs, is very difficult. The velocity field maps provided by Asr et al [15] for a lift-based VAWT are inconclusive, stating that complex flow patterns are observed. Some other studies have presented vorticity maps. We are skeptical about these as these studies are based on 2D modelling (similar to the present study) and representing an inherently 3D phenomena (vorticity) in 2D can be very misleading, and hence, we have not included any vorticity maps here. It is however evident from figure 7(b) that the flow characteristics in the wake region of the VAWT are highly non-uniform and extend multiple VAWT diameters downstream. During the linear acceleration phase, the velocity field seems to be a strong function of time and angular position of the blades, and seems to stabilise during the transition phase.

3.2 Start-up Dynamics of VAWT with Stator

The time-dependant rotational characteristics of the VAWT with the stator blades have been presented in figure 8, where figure 8(a) depicts the angular rotation (θ), while figure 8(b) depicts the rotational speed (ω). It can be seen be seen in both figures 8(a and b) that the start-up dynamics of the VAWT with the stator are qualitatively very similar to the VAWT without the stator. For the first 100s of operation, the VAWT with stator undergoes ~ 133 full revolutions, compared to 60 revolutions for the VAWT without the stator, indicating that the rotational speed of the VAWT with stator is significantly higher. In figure 8(b), it can be clearly seen that the maximum ω of the VAWT reaches 85.3 rpm, which is more than twice the maximum ω for the VAWT without the stator. Hence, it can be concluded that by adding an appropriately designed stator to a drag-based VAWT, the steady rotational speed of the VAWT increases, and thus, the power output of the VAWT also increases.

In terms of the start-up dynamics of the VAWT with the stator blades, we observe the same three zones that we observed earlier in case of VAWT without the stator i.e. linear acceleration, transition and plateau region. The time taken by the VAWT to reach peak ω is 49s, which is slightly more than double the time taken by the VAWT without the stator (23s). Similarly, the VAWT with the stator undergoes 61 full revolutions before achieving peak ω, while the VAWT without the stator underwent 12 full revolutions. This demonstrates that it takes longer for the VAWT with stator to achieve steady rotation, because it has to reach a much higher ω. Further analysing the start-up dynamics of the VAWT with stator with the aim to investigate the reasons behind this delay in reaching steady operation, we observe that ω = 50.8 (59 % of peak) after 5s of operation. Interestingly, the VAWT without the stator also reached 59 % of peak ω after first 5s of operation. At t = 10s, ω = 67.6 (79 % of peak) for the VAWT with stator, while at the same time stamp, the VAWT without stator reached 86 % of peak ω. Further progressing in time, at t = 20s, ω = 79.3 (93 % of peak) for the VAWT with stator, while the VAWT without stator reached 98 % of peak ω. Up to this point in time, the difference in the ratio of instantaneous-to-peak ω between the two VAWT models considered has been < 10 %. At t = 30s, ω = 83.1 (97 % of peak), and at t = 40s, ω = 84.5 (99 % of peak) in case of VAWT with stator. Thus, it is clear that although the time spent by both the VAWT models during linear acceleration is roughly the same, the time spent on the transition to steady operation is significantly different, with VAWT with stator spending 39s, while the VAWT without stator spending just 13s to complete this transition. This will be further analysed later in the study while discussing figure 10.

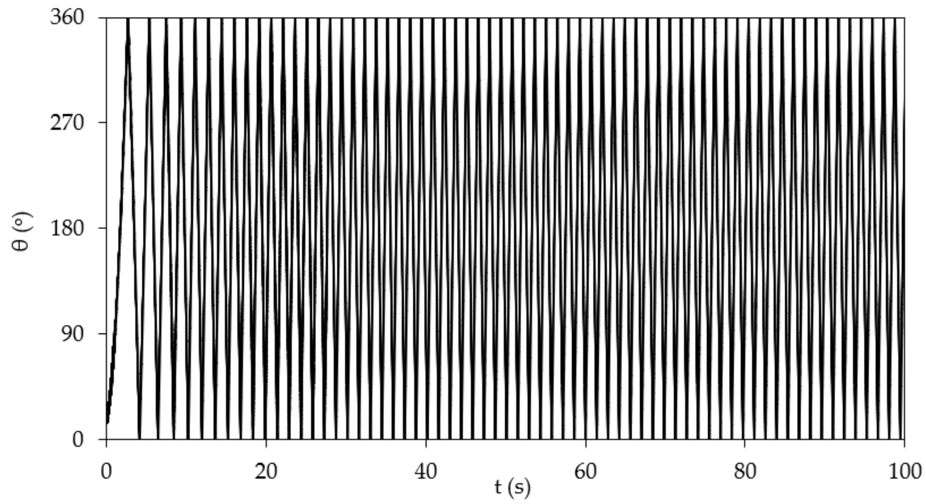

(a)

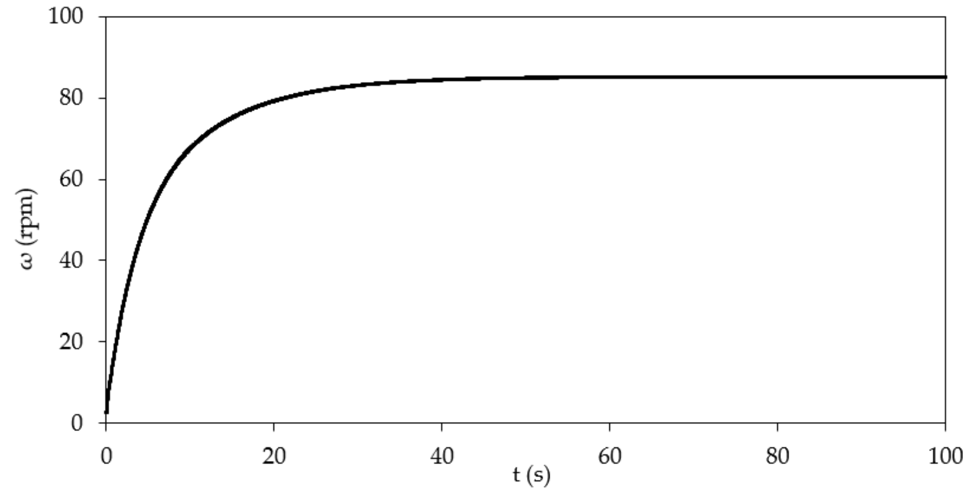

(b)

Figure 8. Rotational characteristics of the VAWT with stator

The flow fields associated with the VAWT model considered here (having stator blades) are shown in figure 9. It can be seen in figure 9(a), in comparison with figure 7(a) regarding the VAWT without the stator, that although the scale of static gauge pressure variations is similar i.e. ~ 110 Pa,g (due to the same wind velocity), it has shifted towards the positive pressure region (higher positive and lower negative pressures). The flow patterns observed in case of VAWT with stator are quite different to the VAWT without stator. It is observed that there exist large areas of negative pressure inside the core region and between top stator blades of the VAWT, which initially start to develop while the VAWT is undergoing linear acceleration. The pressure further drops during the transition phase until it reaches its maximum value at steady operation of the VAWT. The asymmetry between the top and bottom blades is visible again, due to the orientation of the stator blades, with the difference that the stator blades are non-rotating.

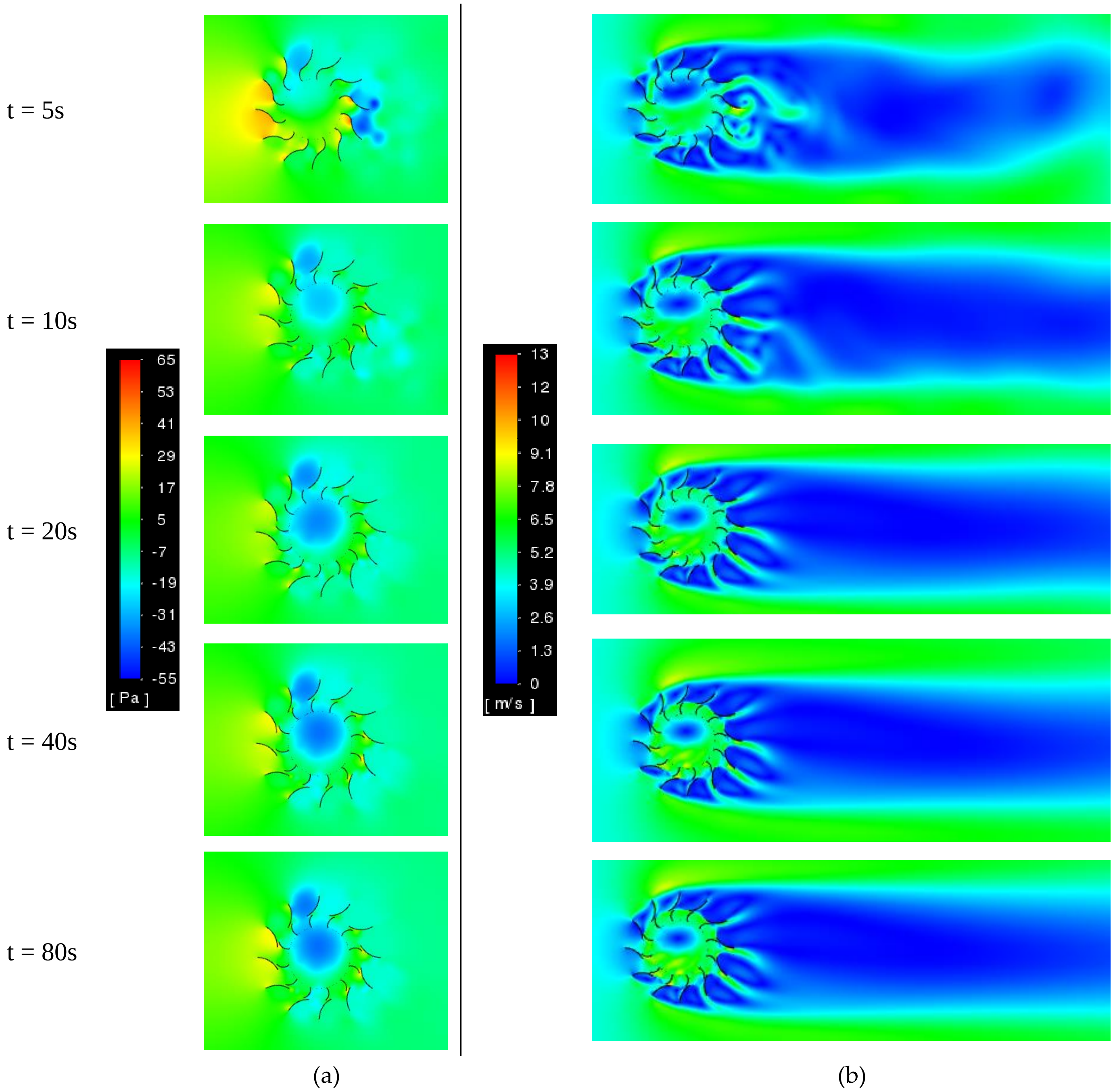

Figure 9. (a) Static gauge pressure and (b) flow velocity magnitude variations in the vicinity of the VAWT with stator

Analysing the flow velocity magnitude field shown in figure 9(b), it can be seen that the flow is significantly more uniform downstream the VAWT, in comparison with the VAWT without the stator blades (figure 7(b)). Hence, the addition of non-rotating stator blades leads towards enhanced structural stability of the VAWT, based on flow uniformity. This must not be confused with higher vibrations in the structure of the VAWT with stator blades due to higher rotational speed (physically observed in lab-based experiments [38-39]). With regards to the start-up dynamics of the VAWT with stator, it is evident that during the linear acceleration phase, as the flow field is constantly developing, the flow is quite non-uniform in the wake region of the VAWT. The flow then stabilises during the transition phase, and eventually reaches a steady condition. In terms of the scale of flow velocity variations, there is negligible difference between the two VAWT models considered in the present study (maximum flow velocity of 12 m/s).

3.3. Start-up Performance Characteristics of VAWTs with and without Stator

After conducting a detailed analysis of the rotational characteristics and the flow fields associated with the two VAWT models considered, it is prudent to investigate time-dependant variations in the conventional performance characteristics of the VAWTs, with special attention to the start-up phases. Thus, figure 10 depicts the variations in Tip Speed Ratio (λ) for both the VAWT models. As λ is dependent on the rotational velocity (ω) of the VAWT (equation 9), the trends are identical to ω variations presented above.

$$\lambda = \frac{\omega R}{V} \quad (9)$$

where R is the outer radius of the rotor blades (m) and V is the wind velocity (m/s). The reason for presenting the variations of λ here is to identify the operational λ of the VAWT at that particular wind velocity. This information is of particular interest because in conventional CFD based studies on VAWTs, where ω is prescribed as a boundary condition, it is a common practise to estimate the operational λ, which corresponds to peak power generation. This estimation is based on numerical investigations over a wide range of prescribed ω. This process can lead towards significant over or under estimation of operational λ. For example, Park et al [51] have carried out steady CFD investigations on the VAWT with stator (same as considered in the present study) and has prescribed $0.1 \leq \omega \leq 0.9$. The operational λ estimated based on the numerical results is 0.5. Gareth [38] has also considered operational λ of 0.5 for the same VAWT. In figure 10 however, it can be clearly seen that the operational λ for the VAWT with stator is 1.5. It is important to note here that both Park et al [51] and Gareth [38] have considered wind speed of 4 m/s, which is quite similar to the wind speed of 4.2 m/s considered in the present study. For the VAWT without the stator, the operational λ has been calculated as 0.7, which is ~ half of the operational λ for VAWT with stator (like ω).

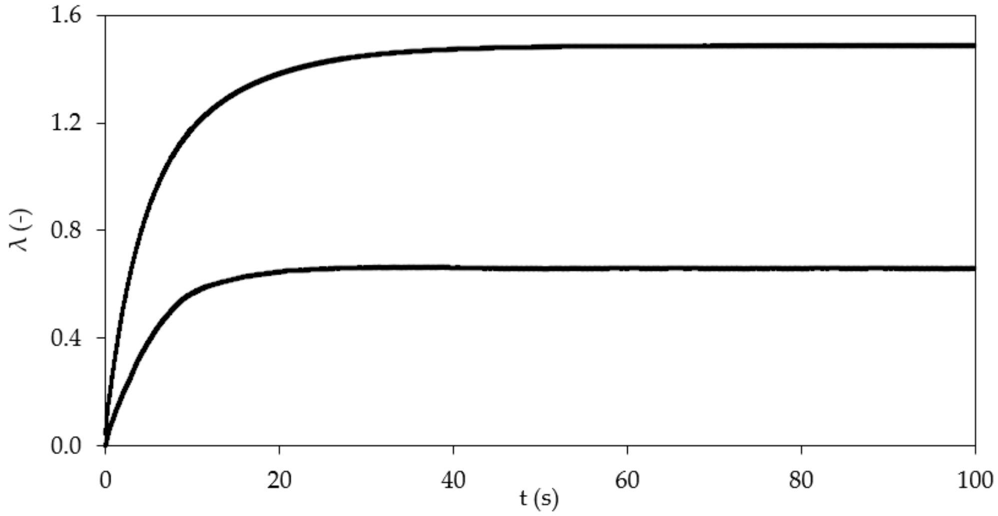

Figure 10. Variations in the Tip Speed Ratio of the VAWTs with and without stator

Concluding the discussions on the start-up dynamics of VAWTs, with and without stator, it is important to highlight the main limitation of the present work. We have not (numerically) considered the generator load, which is applied to the turbine shaft in the real-world, and which potentially affect the operational λ of the VAWT. Without applying the generator load, we get zero average torque (and thus power) output from the VAWT, which is shown in figure 11. It can be seen that, during the steady operation of the VAWTs (plateau region), although we get +ive and -ive instantaneous torque values from both the VAWT models, their average is zero. This has been highlighted by Tigabu et al [24] as well. The instantaneous torque values for the VAWT with stator are considerably higher than for the VAWT with stator (+16.5 Nm compared to +2.1 Nm max), indicating that there is potentially more power generating capability in the former, which can be extracted through the application of brake torque.

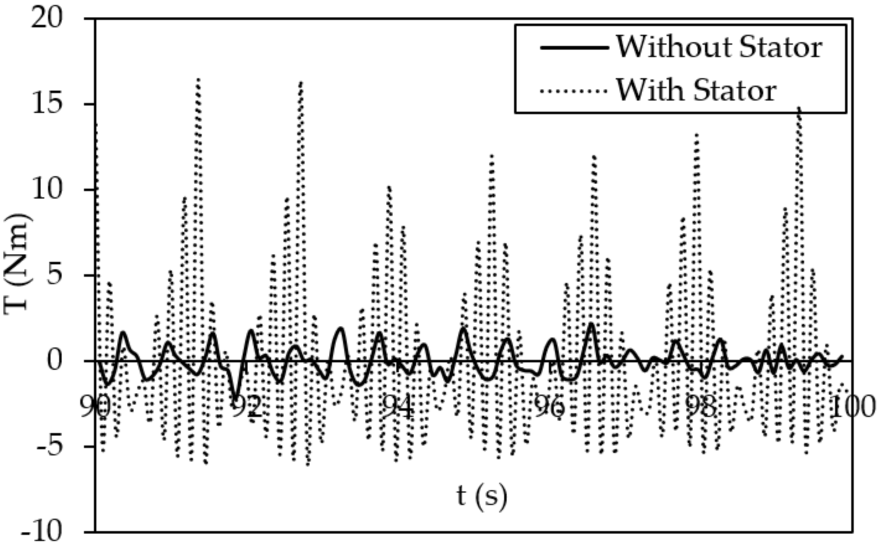

Figure 11. Variations in the torque generated by the VAWTs with and without Stator

4. Conclusions

The start-up dynamics of 12-bladed drag-based VAWT models, with and without the stator blades, have been investigated in the present study. The start-ups of the VAWTs have been numerically simulated, at average UK wind speed, through the use of 6DOF solver in a commercial Computational Fluid Dynamics solver, mimicking flow induced rotation to the VAWTs. We capture time-dependant performance characteristics and local flow features in the vicinity of both the VAWT considered, not only during the start-up phase, but extending to the steady operation of the VAWTs. Based on the detailed results presented, it can be concluded that the addition of appropriately designed stator blades increases the rotational speed, and thus, tip speed ratio and potential power output from the VAWT.

In terms of the start-up, we observe three distinct zones i.e. linear acceleration, transition and steady operation of the VAWTs, irrespective of whether there are stator blades or not. The linear acceleration phase takes roughly the same time, from starting, in both the VAWTs, while the transition phase in case of VAWT with stator is prolonged, as the peak ω is more than double compared to the VAWT without stator. The flow fields associated with rotor only VAWT are significantly more asymmetric, both due to the orientation and the rotation of the blades, leading to pockets of recirculation zones being shed into the wake region of the VAWT.

For the VAWT with stator, as the stator blades are stationary, the intensity of these recirculation zones is less and thus, we observe more uniform flow downstream the VAWT. In either case, the complex flow patterns in the near-wall regions start to develop during the linear acceleration phase, get strengthened during the transition phase, before reaching their maximum values (of corresponding flow parameters) during steady operation of the VAWTs. The operational tip speed ratio of the VAWT with stator, like the rotational speed, is more than double than the VAWT with stator, reaching a value of 1.5.

It is envisaged that this study will pave the way for further scientific investigations on the start-up dynamics of drag-based VAWTs.

Author Contributions: Conceptualization, T.A.; methodology, T.A.; software, T.A.; validation, T.A.; formal analysis, T.A.; investigation, T.A.; resources, T.A..; data curation, T.A.; writing—original draft preparation, T.A. and D.S..; writing—review and editing, T.A., D.S. and D.M..; project administration, T.A and M.A.S. All authors have read and agreed to the published version of the manuscript.

Conflicts of Interest: The authors declare no conflict of interest.

References

1. Du, L.; Ingram, G.; Dominy, R.G. A Review of H-Darrieus Wind Turbine Aerodynamic Research. *Proc. Inst. Mech. Eng. Part C J. Mech. Eng. Sci.***2019**, *233*, 7590-7616.
2. Zhao, Z.; Wang, D.; Wang, T.; Shen, W.; Liu, H.; Chen, M. A Review: Approaches for Aerodynamic Performance Improvement of Lift-Type Vertical Axis Wind Turbine. *Sustain. Energy Technol. Assessments* **2022**, *49*, 101789.
3. Siddiqui, M.S.; Khalid, M.H.; Badar, A.W.; Saeed, M.; Asim, T. Parametric Analysis Using CFD to Study the Impact of Geometric and Numerical Modeling on the Performance of a Small Scale Horizontal Axis Wind Turbine. *Energies* **2022**, *15*, 505.
4. Yang, J.; Fang, Lingqi; Song, D.; Su, M.; Yang, X.; Huang, Lingxiang; Young,; Joo, H. Review of Control Strategy of Large Horizontal-Axis Wind Turbines Yaw System. *Wind Energy* **2021**, *24*, 97-115.
5. Pope, K.; Rodrigues, V.; Doyle, R.; Tsopelas, A.; Gravelsins, R.; Naterer, G.F.; Tsang, E. Effects of Stator Vanes on Power Coefficients of a Zephyr Vertical Axis Wind Turbine. *Renew. Energy* **2010**, *35*, 1043-1051.
6. Tjiu, W.; Marnoto, T.; Mat, S.; Ruslan, M.H.; Sopian, K. Darrieus Vertical Axis Wind Turbine for Power Generation I: Assessment of Darrieus VAWT Configurations. *Renew. Energy* **2015**, *75*, 50-67.
7. Kinzel, M.; Mulligan, Q.; Dabiri, J.O. Energy Exchange in an Array of Vertical-Axis Wind Turbines. *J. Turbul*. **2012**, *13*, 1-13.
8. Dabiri, J.O. Potential Order-of-Magnitude Enhancement of Wind Farm Power Density via Counter-Rotating Vertical-Axis Wind Turbine Arrays. *J. Renew. Sustain. Energy* **2011**, *3*, 043104.
9. Zhipeng, T.; Yingxue, Y.; Liang, Z.; Bowen, Y. A review on the new structure of Savonius wind turbines. *Advanced Materials Research*. **2012**, *608*, 467-478.
10. Asim, T.; Islam, S.Z.; Effects of Damaged Rotor on Wake Dynamics of Vertical Axis Wind Turbines. *Energies*. **2021**, *14*, 7060.
11. Hill, N.; Dominy, R.; Ingram, G.; Dominy, J. Darrieus Turbines: The Physics of Self-Starting. *Proc. Inst. Mech. Eng. Part A J. Power Energy* **2008**, *223*, 21-29.
12. Rossetti, A.; Pavesi, G. Comparison of Different Numerical Approaches to the Study of the H-Darrieus Turbines Start-Up. *Renewable Energy*. **2013**, *50*, 7-19.
13. Somoano, M.; Huera-Huarte, F.J. The Dead Band in the Performance of Cross-Flow Turbines: Effects of Reynolds Number and Blade Pitch. *Energy Conversion and Management*. **2018**, *172*, 277-284.
14. Ebert, P.R.; Wood, D.H. Observations of the Starting Behaviour of a Small Horizontal axis Wind Turbine. *Renewable Energy*. **1997**, *12*, 245-257.
15. Asr, M.T.; Nezhad, E.Z.; Mustapha, F.; Wiriadidjaja, S. Study on Start-up Characteristics of H-Darrieus Vertical Axis Wind Turbines Comprising NACA 4-Digit Series Blade Airfoils. *Energy* **2016**, *112*, 528-537.
16. Rainbird, J. The Aerodynamic Development of a Vertical Axis Wind Turbine. Master's thesis, University of Durham, Durham, UK, **2007**.
17. Jian-Yang, Z.; Lin, J.; Hui, Z. Effect of wind fluctuating on self-starting aerodynamics characteristics of VAWT. *Journal of Central South University*. **2016**, *23*, 2075-2082.
18. Zhu, J.; Tian, C. Effect of Rotation Friction Ratio on the Power Extraction Performance of a Passive Rotation VAWT. *International Journal of Rotating Machinery*. **2019**, *2019*, 6580345.
19. Sun, X.; Zhu, J.; Li, Z.; Sun, G. Rotation improvement of vertical axis wind turbine by offsetting pitching angles and changing blade numbers. *Energy*. **2021**, *215*, 119177.
20. Zhu, J.; Huang, H.; Shen, H. Self-starting aerodynamics analysis of vertical axis wind turbine. *Advances in Mechanical Engineering*. **2015**, *7*, 1-12.
21. Ackermann, T.; Söder, L. Wind Energy Technology and Current Status: *A Review. Renew. Sustain. Energy Rev*. **2000**, *4*, 315-374.
22. Bangga, G.; Hutani, S.; Heramarwan, H. The Effects of Airfoil Thickness on Dynamic Stall Characteristics of High-Solidity Vertical Axis Wind Turbines. *Adv. Theory Simul.* **2021**, *4*, 2000204
23. Dominy, R.G.; Lunt, P.; Bickerdyke, A.; Dominy, J. Self-Starting Capability of a Darrieus Turbine. Proceedings of the Institute of Mechanical Engineering, Part A, *Journal of Power Energy.* **2007**, *221*, 111-120.
24. Tigabu, M.T.; Khalid, M.S.U.; Wood, D.; Admasu, B.T. Some Effects of Turbine Inertia on the Starting Performance of Vertical-Axis Hydrokinetic Turbine. *Ocean Eng.* **2022**, *252*, 111143.
25. Goude, A.; Lundin, S. Forces on a Marine Current Turbine during Runaway. *Int. J. Mar. Energy* **2017**, *19*, 345-356.

26. Zhao, H.; Kang, C.; Ding, K.; Zhang, Y.; Li, B. Transient Startup Characteristics of a Drag-Type Hydrokinetic Turbine Rotor. *Energy Convers. Manag.* **2020**, 223, 113287.
27. Kang, C.; Zhao, H.; Li, B.; Gong, W.; Zhu, Y. Improvement of Startup Performance of the Drag-Type Hydrokinetic Rotor through Two-Stage Configuration. *Ocean Eng.* **2021**, *238*, 109677.
28. Zhao, H.; kang, C.; Ding, K.; Zhang, Y.; Li, B. Transient startup characteristics of a drag-type hydrokinetic turbine rotor. *Energy Conversion and Management*. **2020**, *223*, 113287.
29. Mu, Z.; Tong, G.; Xiao, Z.; Deng, Q.; Feng, F.; Li, Y.; Arne, G.V. Study on Aerodynamic Characteristics of a Savonius Wind Turbine with a Modified Blade. *Energies*. **2022**, *15*, 6661.
30. Altan, B.D.; Atilgan, M. The Use of a Curtain Design to Increase the Performance Level of a Savonius Wind Rotors. *Renew. Energy* **2010**, *35*, 821-829.
31. Golecha, K.; Eldho, T.I.; Prabhu, S.V. Influence of the Deflector Plate on the Performance of Modified Savonius Water Turbine. *Appl. Energy* **2011**, *88*, 3207-3217.
32. Alizadeh, H.; Jahangir, M.H.; Ghasempour, R. CFD-Based Improvement of Savonius Type Hydrokinetic Turbine Using Optimized Barrier at the Low-Speed Flows. *Ocean Eng*. **2020**, *202*, 107178.
33. Hayashi, T.; Li, Y.; Hara, Y. Wind Tunnel Tests on a Different Phase Three-Stage Savonius Rotor. *JSME Int. Journal, Ser. B Fluids Therm. Eng*. **2005**, *48*, 9-16.
34. Su, J.; Chen, Y.; Han, Z.; Zhou, D.; Bao, Y.; Zhao, Y. Investigation of V-Shaped Blade for the Performance Improvement of Vertical Axis Wind Turbines. *Appl. Energy* **2020**, *260*, 114326.
35. Jiang, Y.; He, C.; Zhao, P.; Sun, T. Investigation of Blade Tip Shape for Improving VAWT Performance. *J. Mar. Sci. Eng*. **2020**, *8*, 225.
36. Roy, S.; Saha, U.K. Wind Tunnel Experiments of a Newly Developed Two-Bladed Savonius-Style Wind Turbine. *Appl. Energy* **2015**, *137*, 117–125.
37. Asim, T.; Islam, S.Z.; Hemmati, A.; Khalid, M.S.U. A Review of Recent Advancements in Offshore Wind Turbine Technology. *Energies* **2022**, *15*, 579.
38. Colley, G. Design, Operation and Diagnostics of a Vertical Axis Wind Turbine. PhD thesis, Univ. Huddersfield, Huddersfield, UK, 2012.
39. Park, K.S.; Asim, T.; Mishra, R. Computational fluid dynamics based fault simulations of a vertical axis wind turbines. *Journal of Physics: Conference Series*. **2012**, *364*, 012138.
40. Shahzad, A.; Asim, T.; Mishra, R.; Paris, A. Performance of a vertical axis wind turbine under accelerating and decelerating flows. *Procedia CIRP*. **2013**, *11*, 311-316.
41. Mohamed, F.; Park, K.S.; Pradhan, S.; Mishra, R.; Zala, K.; Asim, T.; Al-Obaidi, A. The effect of blade angles of the vertical axis wind turbine on the output performance. *Proceedings of 27th International Congress of Condition Monitoring and Diagnostic Engineering*. **2014**, Brisbane, Australia.
42. Park, K.S.; Asim, T.; Mishra, R. Numerical Investigations on the Effect of Blade Angles of a Vertical Axis Wind Turbine on its Performance Output. *International Journal of Condition Monitoring and Diagnostic Engineering*. **2015**, *18*, 3-10.
43. Asim, T.; Mishra, R.; Kaysthagir, S.N.; Aboufares, G. Performance comparison of a vertical axis wind turbine using commercial and open source computational fluid dynamics based codes. *Proceedings of 5th International Conference on Jets, Wakes and Separated Flows*. **2015**, Stockholm, Sweden.
44. Zahariev, M.; Asim, T.; Mishra, R.; Nsom, B. Effects of blade tapering on the performance of vertical axis wind turbines analysed through advanced visualization techniques. *International journal of Condition Monitoring and Diagnostic Engineering*. **2019**, *22*, 69-74.
45. Aboufares, G.; Zala, K.; Mishra, R.; Asim, T. Effects of Sand Particle Size on the Performance Characteristics of a Vertical Axis Wind Turbine. *Proceedings of 6th International and 43rd National Conference on Fluid Mechanics and Fluid Power*. **2016**, Allahabad, India.
46. Singh, D.; Aliyu, A.M.; Charlton, M.; Mishra, R.; Asim, T.; Oliveira. A.C.; Local multiphase flow characteristics of a severe-service control valve. *Journal of Petroleum Science and Engineering*. **2020**, *195*, 107557.
47. Singh, D.; Charlton, M.; Asim, T.; Mishra, R.; Quantification of additive manufacturing induced variations in the global and local performance characteristics of a complex multi-stage control valve trim. *Journal of Petroleum Science and Engineering*. **2020**, *190*, 107053.
48. Versteeg, H.K.; Malalasekera, W. An Introduction to Computational Fluid Dynamics: The Finite Volume Method. 2nd ed. **2007**. Pearson.
49. Spalart, P.R. Trends in Turbulence treatments. *Fluids 2000 Conference and Exhibit*. **2000**, Denver, USA.
50. ANSYS, Inc. ANSYS Fluent User's Guide, Release 2021 R2, **2021**.
51. Park, K.S.; Asim, T.; Mishra, R.; Pradhan, S. Condition based monitoring of vertical axis wind turbines using computational fluid dynamics. *Proceedings of 39th National Conference on Fluid Mechanics and Fluid Power*. **2012**, Surat, India.